Novel Solar Reactor for Studying Ultrafast Gas–Solid Reactions Above 2,000 K

E. Steiner, J. Ganz, A. Meier, and M. Sturzenegger
High-Temperature Solar Technology, Paul Scherrer Institut, 5232 Villigen PSI/Switzerland

A novel solar chemical reactor has been designed and tested for kinetic experiments with μm-sized metal oxide particles. The solar reactor is essentially a tubular reactor with a continuous feed of particles suspended in a carrier gas. The suspension is electrically preheated in the back part of the solar reactor. Chemical conversion occurs in the high-temperature zone in the front part of the solar reactor where concentrated solar radiation enters the reactor through a quartz window. Under typical operating conditions, the particle residence time in the high-temperature zone was estimated to be 50 ms. Reduction of manganese iron oxides showed that flux-density distributions of 450 to 770 $W \cdot cm^{-2}$ produced maximum particle temperatures of 2,200 K. Chemical reactivity studies also revealed that quenching is insufficient for very reactive materials. Therefore, an alternative quench device has been tested at room temperature and is discussed here.

Introduction

The reduction of metal oxides by means of concentrated solar radiation is a key step in closed-loop processes aimed at a sustainable hydrogen production (Funk, 1975; Nakamura, 1977; Steinfeld et al., 1998). It is essentially the conversion of the intermittent solar radiation into storable chemical energy. The reactions proposed include, among others, the reduction of zinc oxide (ZnO) (Palumbo et al., 1998), iron oxide (Fe_3O_4) (Nakamura, 1977; Tofighi and Sibieude, 1984), mixed iron oxides $(M_xFe_{1-x})_3O_4$ (Kuhn et al., 1995; Nüesch, 1994), and manganese oxide (Mn_2O_3) (Sturzenegger et al., 1999; Sturzenegger and Nüesch, 1999). Thermally induced reduction of these oxides occurs at temperatures above 2,000 K and ensures conversion of radiant energy into chemical energy with exergy efficiencies up to 70% (Sizmann, 1991; Steinfeld and Schubnell, 1993).

Kinetic studies on the decomposition of these metal oxides are a prerequisite for assessing their potential for solar applications and to design and up-scale solar chemical reactors. Due to the high reaction temperatures and because inductive heating cannot be applied to nonmetallic materials, radiant heating by means of concentrated solar radiation is proposed to conduct such studies. Concentrating solar light by a factor of 5,000 provides straightforward access to reaction temperatures in the range of 2,500 K. Bulk samples with an area of several tens of cm^2 can be heated to such temperatures within seconds, and temperatures may drop to ambient within a few millimeters at the border of the irradiated area. Even higher heating rates can be obtained for particulate samples.

Kinetic studies on bulk samples

Möller and Palumbo (2001a,b) determined the reduction kinetics of pressed ZnO powder exposed to direct solar radiation at temperatures between 1,950 and 2,400 K. They determined the relationship between mass flux and temperature, and derived an Arrhenius-type expression for the reduction kinetics. To study the solar thermal reduction of molten iron oxides Tofighi (1982) developed various experiments that allow for working under defined atmospheres and quenching of the samples at various rates. However, the time dependency of the reduction has to be derived from a series of discrete measurements. Frey et al. (2001) fabricated a solar reactor for studying the reduction of mixed iron oxides at temperatures between 2,000 and 2,200 K under defined atmospheres. The reactor design allows for on-line mass spectrometry to monitor the oxygen evolution in the course of the reaction, and it includes a quench device for freezing the

Correspondence concerning this article should be addressed to M. Sturzenegger.
Current addresses of: E. Steiner, AAC Infotray AG, Neumühlestr. 42, 8406 Winterthur/Switzerland; J. Ganz, AWTEC, AG für Technologie und Innovation, Leutschenbachstr. 42, CH-8050 Zürich/Switzerland.

high-temperature composition of the sample at the end of the experiment. The temperatures of the solar irradiated samples can be directly measured, for example, by flash-assisted multi-wavelength pyrometry (Tschudi and Schubnell, 1999), due to the optical access to the sample during the entire measurement. Quantitative kinetic information is obtained for a given temperature by a single measurement.

Particulate samples

Particulate samples have a higher surface-to-volume ratio than bulk samples, which in general leads to shorter reaction times. Very small particles provide a very large surface area, and exposure to a high-intensity radiation field, such as concentrated solar radiation, ensures an efficient heat and material exchange between gaseous and condensed phase (Yuen et al., 1986). This suggests that the observed overall reduction kinetics is controlled by the chemical kinetics, thus representing the maximum possible conversion rates.

The short reaction times—μm-sized metal oxide particles, for example, are expected to react within a few milliseconds—require different reactor concepts. More importantly, working with particles impedes a rigorous kinetic analysis due to the size distribution of real materials. To solve that latter problem, Raghunathan et al. (1993) interfaced their ingenious experiment for kinetic studies in the time scale of 10 to 100 ms with a cascade impactor for *in situ* separation of the reacted particles. Samples from the cascade plates were analyzed after the measurement, and the decomposition kinetics was quantitatively determined. Since they are using a conventional Lindberg furnace, its upper working temperature is limited to about 1,700 K.

Early attempts to study fast gas/solid reactions under concentrated solar radiation were reported by Kuhn et al. (1995). Metal oxide particles were dispersed in a carrier gas, and the suspension was injected into a quartz tube reactor that was positioned in the focal plane of the solar furnace. The particles were heated by direct absorption of concentrated solar radiation; their residence time in the radiant field could be varied between 0.1 and 0.5 s by adjusting the gas flow rate. Experiments with mixed iron oxides showed that flux densities of 200–250 $W \cdot cm^{-2}$ induce complete conversion of hematite-type $(Fe_{0.9}Mn_{0.1})_2O_3$ into spinel-type $(Fe_{0.9}Mn_{0.1})_3O_4$ at approximately 1,700 K. These flux densities, however, did not produce substantial amounts of the desired mangano-wustite $(Fe_{0.9}Mn_{0.1})O$. Furthermore, operation of the solar reactor was plagued by particle deposition onto the quartz tube.

In this article we describe the design, the main features, and the characteristics of a novel solar reactor called CAIRO (acronym for chemical axial inlet radial outlet). It was designed to overcome the drawbacks of the previously mentioned quartz tube reactor and to gain further insight in the reduction kinetics of particulate spinel-type mixed iron oxides $(Fe_{1-x}M_x)_3O_4$ to wustite-type $(Fe_{1-x}M_x)O$, where M denotes Mn or Mg.

Design of the Solar Chemical Reactor

The concept of the solar reactor CAIRO was decisively directed by the main goal of the research campaign, namely to demonstrate the feasibility of chemical transformations at temperatures above 2,000 K. It is based on entraining μm-sized particles into a gas stream and exposing the gas/solid suspension to concentrated solar radiation. The particles directly absorb the radiant energy, which induces heating and chemical conversion. Further details on the theory, design, and applications of solar "powder cloud" reactors can be found elsewhere (Ganz, 1996; Ganz et al., 1999; Hunt, 1982; Hunt et al., 1986). In comparison to the previously described quartz tube reactor (Kuhn et al., 1995), three major changes were introduced:

1. The reactor CAIRO is equipped with a compound parabolic concentrator (CPC), that is, a nonimaging secondary concentrator (Welford and Winston, 1989). The CPC has a diameter of 45.7 mm at its entrance and a diameter of

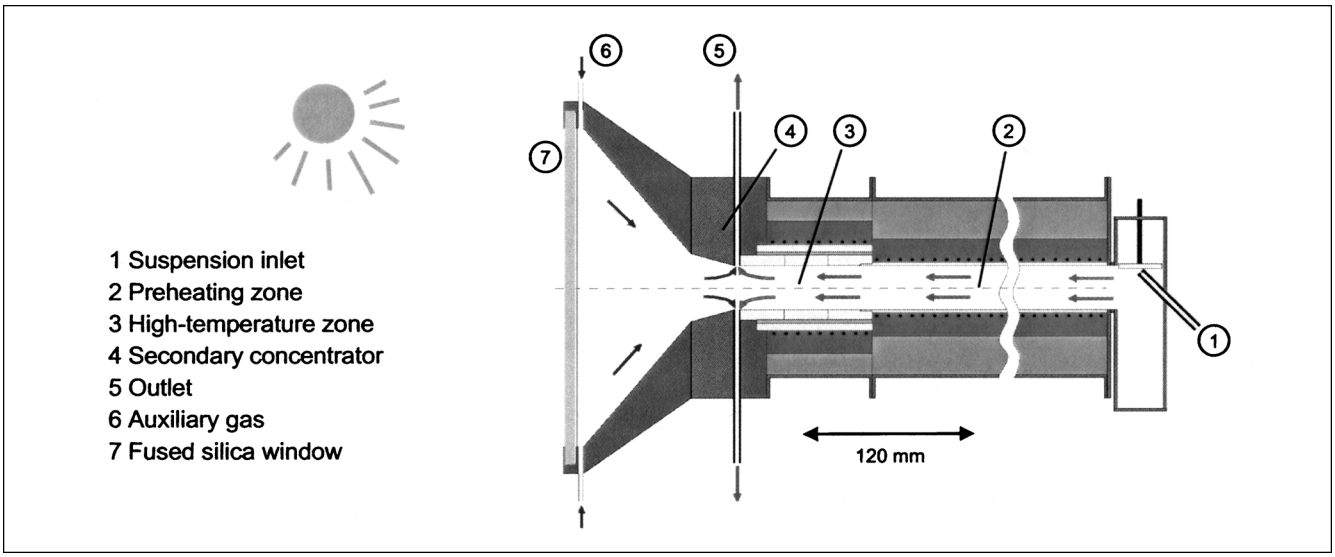

Figure 1. The solar reactor CAIRO.

30 mm at its outlet plane. It was designed to concentrate the solar radiation supplied by the solar furnace by a factor of approximately 1.8 to yield flux densities close to 700 $W \cdot cm^{-2}$. According to a simple model for particles in a radiation field, such flux densities yield stagnation temperatures between 2,600 and 3,000 K (see later in text).

2. The concept of "hot particles–cold walls" was abandoned, because the dimension of the particle cloud and its optical thickness are not sufficient to allow establishment of a substantial temperature gradient between the center of the cloud and the reactor wall (Ganz et al., 1999). Now, the zirconia-lined high-temperature zone is intentionally heated by the solar radiation to minimize heat loss from the particles to the wall.

3. The counterflow between the incoming solar radiation and the particle/gas suspension establishes a temperature gradient through the opaque particle cloud. Thus, reradiation losses to the environment determined by the mean temperature of the particle cloud are lower, and consequently the thermal efficiency is increased in comparison to a cavity absorber where essentially the entire interior reactor surface is at the maximum working temperature (Ganz, 1996).

The salient features of the solar reactor CAIRO are sketched in Figure 1. A rotating brush powder cloud generator (not shown in the figure) in the rear part of the reactor generates the particle/gas suspension that is continuously fed through a nozzle and impinges on an inclined plate (1). Large particles or conglomerates deposit in the sedimentation chamber while the homogenized particle cloud proceeds toward the front part of the reactor. It first passes the preheating zone (2) at 1,273 K, before it reaches the high-temperature zone (3), where the concentrated solar radiation induces the chemical transformation. The high-temperature zone consists of three cylindrical zirconia tubes (Zircar insulation type FBD, working temperature 2,450 K). The tubes have a length and an inner diameter of 32 mm each; the outer diameter is 57 mm. They are worked into an alumina tube, which is enclosed by an electric heater for preheating the high-temperature zone. Preheating is needed to lessen thermal shocks during the startup phase when concentrated solar radiation rapidly heats the cold walls; thus, it extends the lifetime of the zirconia elements.

Once the particles have passed the high-temperature zone, they are quenched while radially leaving the reactor through thin openings between the high-temperature zone and the water-cooled backside of the CPC (5). Quenching is enhanced by the cold auxiliary gas (inlet at position 6), which also helps to keep the window (7) and the CPC (4) clean. The particles are collected on filters and subject to further characterization.

Design of the reactor outlet

Particular attention was given to the design of the reactor outlet. It is located between the water-cooled CPC and the zirconia tube enclosing the high-temperature zone (see Figure 1). While passing the outlet channels, the suspension is quenched on the rear side of the water-cooled CPC and additionally by the cold auxiliary gas. Computational fluid dynamics (CFD) simulations confirmed that the design of the outlet, in conjunction with the applied flow rates of the carrier gas and the auxiliary gas, has a decisive influence on the gas flow pattern and, therefore, on the maximum working temperature as well as on the successful prevention of particle deposition on the CPC and on the window.

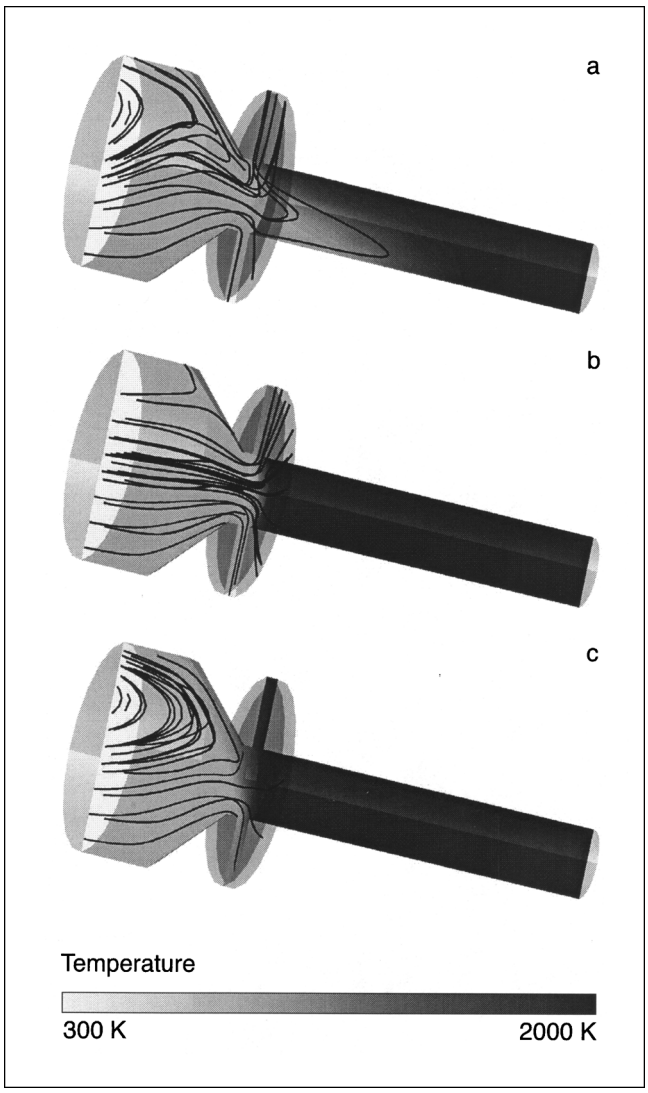

Figure 2. 3-D Representation of the CFD calculations for three different gas flow conditions.

Streamlines visualize the flow in the forefront of the solar reactor. The gray scale in the vertical mirror plane refers to the calculated temperatures. For details see text.

The behavior of the gas flows was assessed and visualized by CFD calculations for a model with dimensions identical to those of the solar reactor, assuming adiabatic reactor walls. The carrier gas was fed with an inlet temperature of 2,000 K and a uniform inlet velocity distribution (corresponding to a specified mass flow rate) to the high-temperature zone. The auxiliary gas was at room temperature, and it entered the reactor through the aperture (pressure boundary, Dirichlet boundary condition). The mixed gas exited the reactor in the radial direction through four identical sectors with an outer radius of 45 mm and a width of 5 mm at a specified mass flow rate (mass flow boundary, Neumann boundary condi-

Table 1. Input Parameters for the CFD Calculations

Figure No.	Gas (Air) Flow Conditions: Carrier Gas Inlet Velocity u ($m \cdot s^{-1}$)	Carrier Gas Flow ($L \cdot min^{-1}$)	Auxiliary Gas Flow ($L \cdot min^{-1}$)	k-ϵ Turbulence Model: k ($m^2 \cdot s^{-2}$)	ϵ ($m^2 \cdot s^{-3}$)
3a	0.1	0.58	5.8	3×10^{-4}	5.77×10^{-4}
3b	0.5	2.9	5.8	7.5×10^{-3}	7.22×10^{-2}
3c	1	5.8	5.8	3×10^{-2}	5.77×10^{-1}
Remarks	Radial inlet velocity components $v = w = 0\ m \cdot s^{-1}$ Inlet temperature $T = 2{,}000$ K Tube diameter $D = 0.03$ m Density $\rho_{2,000K} = 0.174\ kg \cdot m^{-3}$ Density $\rho_{273K} = 1.275\ kg \cdot m^{-3}$		$\dot{V} = uA = u\frac{\pi D^2}{4}\frac{\rho_{2,000K}}{\rho_{273K}}$	$k = 0.03u^2$	$\epsilon = \frac{k^{1.5}}{0.3D}$

tion). The complete set of input parameters is listed in Table 1. Figures 2a–2c show the streamlines in the front part of the reactor and in the radial outlet plane, as well as the temperature distribution in the vertical mirror plane for three different flow conditions. From these figures we can appreciate that under all conditions buoyancy effects will force hot gas to exit the reactor through the upper part of the outlet while colder auxiliary gas will exit through the lower part of the outlet. The asymmetry is less pronounced the closer to unity the ratio of carrier gas to auxiliary gas is. Figure 2a was obtained with a carrier gas flow rate of 0.58 $L \cdot min^{-1}$ and an auxiliary gas flow rate of 5.8 $L \cdot min^{-1}$. Such gas-flow rates are not suitable because the cold auxiliary gas would deeply penetrate into the high-temperature zone, thus substantially lowering the maximum working temperature. In addition, recirculation occurs in the hotter upper part, and undesired particle deposition onto the CPC or the window is expected. An almost optimal flow pattern is obtained when the auxiliary gas flow is reduced to values two times as high as the carrier gas flow (see Figure 2b). Penetration of cold auxiliary gas into the high-temperature zone of the reactor is substantially reduced. The streamlines indicate that the suspension will exit the reactor through the outlet and that the CPC will stay clean. When the carrier gas flow equals the auxiliary gas flow at a rate of 5.8 $L \cdot min^{-1}$, penetration of cold gas into the high-temperature zone is eliminated. However, recirculation of cold auxiliary gas in front of the aperture forces the particles to exit the reactor through the aperture, and particle deposition onto the CPC or the window is expected (see Figure 2c). The CFD calculations indicate that stable operation of such a reactor should be possible, though the regime with regard to flow rates will be very narrow.

The realized outlet geometry consists of four triangles with a maximum depth of 4 mm at the corner where the flow enters the copper tubing, which has an inner diameter of 4 mm (see Figure 3). The width of the slit between the zero level and the opposite wall of the high-temperature zone is 5 mm.

Modeling and Experimentation

CFD Calculations. Computational fluid dyamics (CFD) calculations were performed with a general-purpose CFD code, CFX-F3D (Anonymous, 1995).

Temperature Calculations. To calculate sample temperatures for heating and stagnation periods, a simple heat-balance model was developed where the heating power equals the difference between the incident and the thermally emitted radiant power (see Eq. 1). The energy consumed by the reduction of the oxide was neglected, since the reaction enthalpy accounts for less than 0.1% of the incident radiant power. The shape of the irradiated particles was approximated by spheres with a radius, r, of 2.5 μm, and only radiant heat transfer was taken into account. Furthermore, the particles were considered to be Lambertian gray bodies with constant identical absorptivity and emissivity ($\alpha = \epsilon$)

$$\rho V c_p \frac{dT}{dt} = \alpha I A_i - \epsilon\sigma T(t)^4 A_0 \qquad (1)$$

The density ρ and the mean value c_p for the heat capacity of the compounds $(Fe_{1-x}M_x)_3O_4$ and $(Fe_{1-x}Mx)O$ were set equal to 5,000 $kg \cdot m^{-3}$ and 800 $J \cdot kg^{-1} \cdot K^{-1}$, respectively (Barin, 1995); V is the volume of the sphere. The term $\epsilon\sigma T(t)^4 A_0$ accounts for the thermally emitted radiation. The emissivity, ϵ, is set to 1, and the Stefan-Boltzmann constant σ equals 5.670×10^{-8} $W \cdot m^{-2} \cdot K^{-4}$; T is the absolute temperature, and A_0 the surface area of the sphere. Since the sample surface is assumed to be Lambertian, the absorbed radiant power equals $\alpha I A_i$. The absorptivity α was assumed to equal 1, I is the flux density measured in the plane of the CPC, and A_i is the irradiated surface. Calculations with A_i equal to the projection of a sphere ($A_i = r^2\pi$) only take into account direct absorption of concentrated solar radiation through the CPC, but neglect thermal emission of the hot walls into the reaction zone. Calculated heating rates and stagnation temperatures therefore represent the lower limit for radiant heating. On the other hand, if A_i equals the total surface ($A_i = 4r^2\pi$), the calculations are based on the assumption that reflected and thermally emitted radiation from other particles and from the hot walls of the high-temperature zone contribute to particle heating. However, since the powder cloud is visually thin, this contribution is considered to be small, and, therefore, these calculations yield the upper temperature limit for radiant heating. Consequently, the calculations where A_i equals the surface of a half sphere ($A_i = 2r^2\pi$) are considered to be a good approximation.

Cold Experiments. A quadrupole mass spectrometer (MS Cube, Balzers) was employed to probe the gas flow in the high-temperature zone at room temperature. Inert gas (nitrogen >99.999%) representing the carrier gas was fed from the back of the reactor, while oxygen (> 99.5%) representing the auxiliary gas was fed through the auxiliary gas

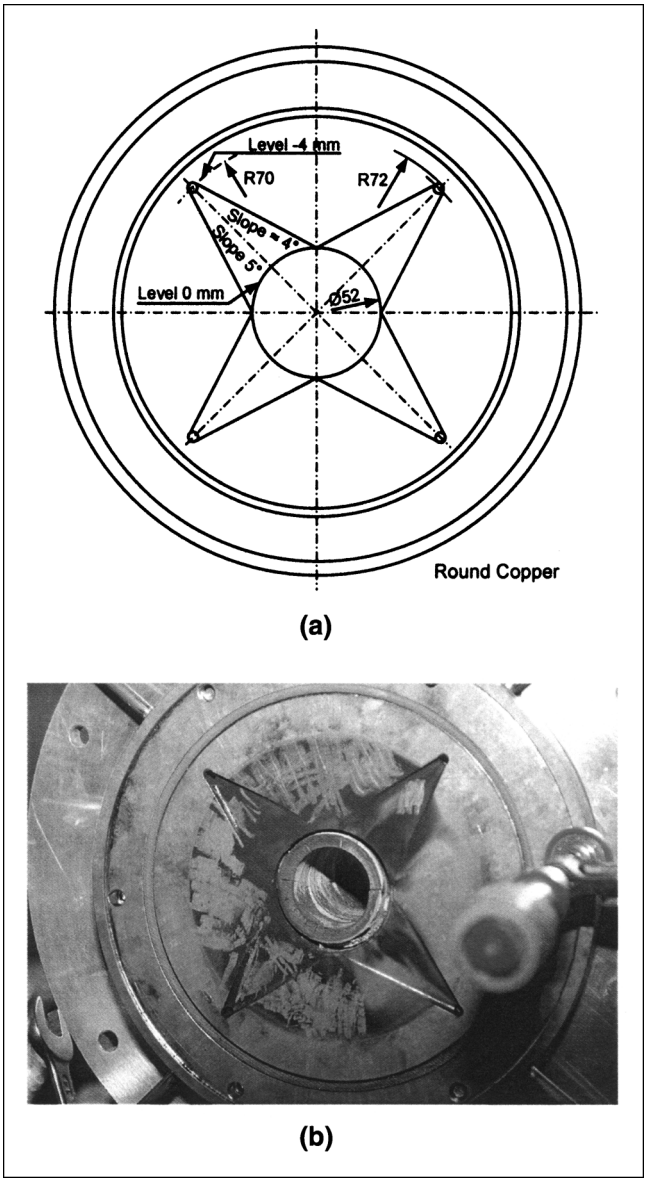

Figure 3. (a) Technical drawing, and (b) photograph of the realized outlet geometry on the backside of the water-cooled CPC.

inlet. The gas composition was measured in the axial center of the high-temperature zone at various positions along the reactor axis.

Solar Experiments. Solar experiments were conducted in the 15-kW high-flux solar furnace at the Paul Scherrer Institute (PSI) (Ries and Schubnell, 1990). It is a two-stage concentrator system consisting of a sun-tracking heliostat with an area of 51.8 m^2 and a stationary parabolic dish with an area of 5.7 m^2. Their focal lengths are 100 m and 1.93 m, respectively. The concentrating system delivers up to 15 kW with a peak concentration ratio of 4,500 suns. A venetian blind-type shutter located between the heliostat and the concentrator controls the power delivered to the reactor. Power flux densities were measured optically by recording the image of the sun on a white Lambertian target by a calibrated charge-coupled device (CCD) camera. The CCD camera is also used to continuously monitor the position of the reactor relative to the flux map, so that the regions of maximum flux intensity are intercepted.

Besides flux measurements, the startup procedure also included preheating of the reactor to reduce thermal stress on the ceramics. Both the preheating zone and the high-temperature zone were electrically heated, the former to 1,273 K, the latter to 1,073 K. During the experiments, power to the preheating zone was fixed, while the heating of the high-temperature zone was reduced to less than 20% of its initial value.

Typically, experiments were conducted at a carrier gas flow of 12.5 $L \cdot min^{-1}$ (fed at STP at position 1 in Figure 1) and a quench gas flow of 25 $L \cdot min^{-1}$ (fed at STP at position 6). The system was kept at atmospheric pressure. The oxygen partial pressure was varied between 0.1 mbar (nitrogen $> 99.999\%$) and 200 mbar (synthetic air). A particle feeder that was developed in-house was employed to produce the gas–solid suspensions. Pressure pulses generated by instabilities of the feeding system were minimized by a straight connection between the feeder and the suspension inlet and by mounting an impinging plate right after the inlet. Due to these measures, pulses were sufficiently reduced to avoid particle deposition on the CPC or on the quartz window. The mass load ratio of the solid/gas suspension was about 0.02 kg powder per kg carrier gas. Product samples were taken at two positions: (1) most of the products were collected on a filter after the suspension had left the reactor system; (2) smaller amounts of samples were collected from deposits at the backside of the water-cooled CPC.

Preparation of the Oxides. $(Fe_{0.9}Mn_{0.1})_3O_4$, $(Fe_{0.9}Mg_{0.1})_3O_4$, and MnO_2, respectively, were used as starting material for the solar experiments. The mixed iron-oxide powders were prepared from the corresponding bimetallic oxalate precursors (Wickham, 1969). The precursors were converted to the corresponding oxide by decomposing them at 1,173 K under a dynamic vacuum. Subsequent oxidation/heating at 873 K for 1 h under a H_2O-H_2 atmosphere ($H_2O/H_2 = 10.8$ vol %/6.2 vol %) in N_2 produced the final products, namely single-phase, spinel-type oxides $(Fe_{0.9}M_{0.1})_3O_4$. MnO_2 (Puriss, Fluka) was used as it was received. The medium diameter of the starting material was determined to be between 4 and 8 μm.

Sample Analysis. Phase analyses were established by means of powder X-ray diffractometry (Philips X'Pert MPD with Cu K_α radiation) and high-temperature powder X-ray diffractometry (Büehler HT-chamber HDK 2.0). Chemical compositions were determined by means of thermogravimetry (Netzsch STA 409) and water splitting analysis (Ehrensberger et al., 1996). In the procedures to calculate the composition, the molecular weights of the compounds were normalized to 1 mole metal cation(s); Mn_3O_4, for example, was treated as $Mn_1O_{1.33}$, which corresponds formally to 1/3 Mn_3O_4. Such an approach generates a one-to-one relation between the conversion (in %) and the amount of each phase (in mol %). Particle-size distribution and mean particle size of the particulate materials were determined in ethanol by a HORIBA laser diffraction analyzer, LA-500. The morphology of the particles was analyzed by means of a scanning electron micrograph (Zeiss).

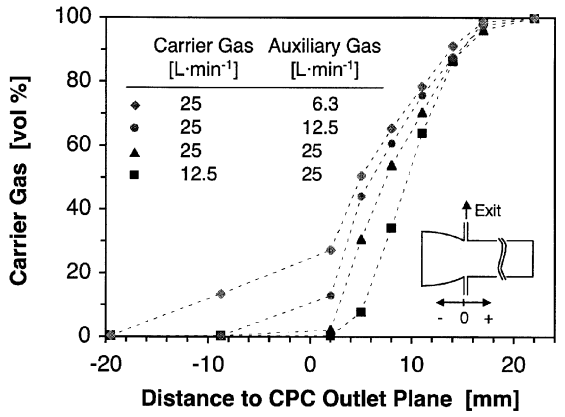

Figure 4. Carrier gas concentration profile in the region of the CPC; all measurements were conducted at room temperature.

Results and Discussion

Characterization of the solar reactor

To validate the CFD calculations, the gas-flow pattern in the high-temperature zone was experimentally investigated at room temperature by gas-phase analysis. Figure 4 displays the results of four measurements with gas-flow rates similar to those employed during experiments in the solar furnace. They show that a portion of the carrier gas is entering the CPC when the flow ratio between carrier gas and auxiliary gas is higher than or equal to 2. If the ratio between carrier gas and auxiliary gas-flow rates is less than or equal to 1, a significant amount of auxiliary gas is penetrating into the reaction zone.

Estimates on the irradiation-limited stagnation temperatures were derived from both flux-density measurements and a simple heat balance model. Figure 5 shows the flux density distribution measured in the focal plane of the solar furnace (at the CPC entrance) at a direct normal insolation of 794 $W \cdot m^{-2}$. Flux densities ranged from 364 $W \cdot cm^{-2}$ in the center of the spot to 310 $W \cdot cm^{-2}$ at the circumference of the CPC entrance. The flux densities in the outlet plane of the CPC, that is, at the front of the high-temperature zone, are plotted in Figure 6. Flux densities of 770 $W \cdot cm^{-2}$ were measured in the center; the flux densities still exceeded 400 $W \cdot cm^{-2}$ close to the reactor wall. Stagnation temperatures were calculated from Eq. 1 for the case that the incoming solar radiation equals the thermally emitted radiation. Figure 7 displays calculated stagnation temperatures as a function of the flux densities with the irradiated area A_i as a parameter. As mentioned earlier, we assume that the real situation is best described by the assumption that half of the particle surface area receives concentrated radiation. Since μm-sized particles have surface-to-volume ratios as high as 10^6 m^{-1}, radiant heat transfer is very effective and stagnation temperatures are reached within a few milliseconds (see Figure 8). Based on the measured 2-D flux-density distribution and on the information that 450 $W \cdot cm^{-2}$ are sufficient to achieve stagnation temperatures of 2,500 K, we conclude that 85% of the solar flux density in the outlet plane of the CPC is sufficient to heat particles to temperatures above 2,500 K within a few milliseconds.

Exposure of particles to different flux densities as it occurs in the solar reactor or when comparing experiments under different solar insolations might be a concern in view of chemical investigations. Figure 7, however, illustrates that the variation in the stagnation temperature is less than 15% for most situations. We assume that this value represents an upper limit for different experiments. For a single experiment, real temperature differences will be smaller due to convective heat-transfer processes. A real disadvantage of this reactor concept is the fact that absolute particle temperatures can hardly be measured by any experimental means.

To allow for semiquantitative interpretation of the experiment, the particle residence time in the high-temperature zone was estimated. Since the particles have a mass of only 0.3 ng, we assumed them to be entrained by the carrier gas

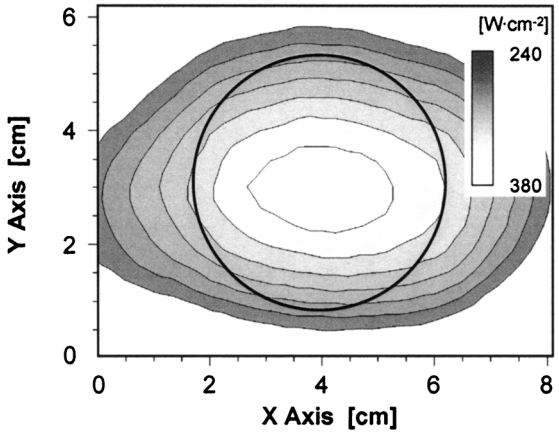

Figure 5. 2-D Solar flux-density distribution (in $W \cdot cm^{-2}$) measured in the focal plane of the high-flux solar furnace at PSI at a direct normal insolation of 794 $W \cdot cm^{-2}$; the circle with a diameter of 45.7 mm represents the entrance of the CPC.

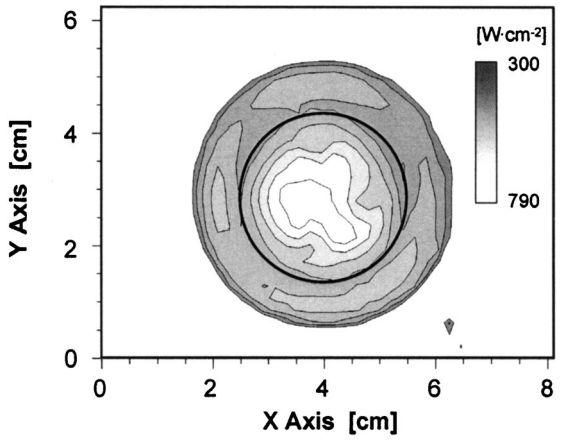

Figure 6. 2-D Solar flux-density distribution (in $W \cdot cm^{-2}$) measured in the outlet plane of the CPC; the circle with a diameter of 30 mm represents the outlet plane of the CPC.

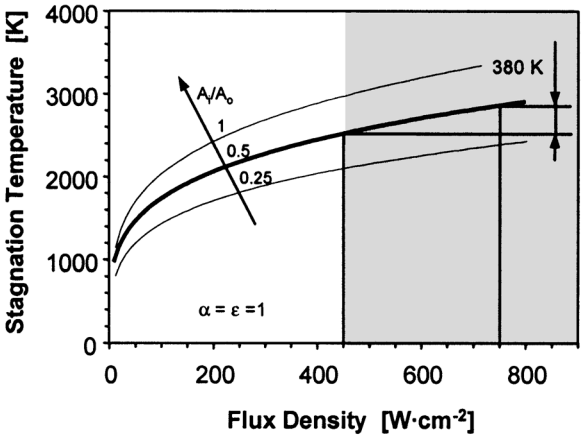

Figure 7. Calculated stagnation temperatures for a black body as a function of the (solar) flux density and of the irradiated surface area, A_i; for details see text.

and to have the same velocity as the gas. The preheated carrier gas was assumed to enter the high-temperature zone with a temperature of 1,273 K and to reach equilibrium with the wall at a temperature of 2,273 K right behind the plane of the CPC after 96 mm. Under the assumption of a linear temperature profile and a cross-section area of 7.1 cm^2, and for a gas flow of 12.5 L·min^{-1}, the time needed to pass the hot reaction zone is calculated to be 52 ms. Under the extreme assumption of instantaneous heating of the gas entering the high-temperature zone, the minimum residence time is lowered to 40 ms. From these calculations, we estimate the residence time of the particles in the high-temperature zone to be about 50 ms.

Experiments under concentrated solar radiation

CFD calculations indicated that the gas-flow rates have a strong influence on the flow pattern in the transition zone between the CPC and the high-temperature zone. Variations of the carrier gas flow and the auxiliary gas flow, respectively, confirmed the expected influence. It turned out that a carrier gas flow of 12.5 L·min^{-1} and an auxiliary gas flow of 25 L·min^{-1} enabled continuous operation of the reactor for up to 90 min without particle deposition on the CPC or on the window. This corresponds well with the CFD calculations. No failures occurred during more than 15 h of operation in the solar furnace with 11 startups. In combination with the pre-

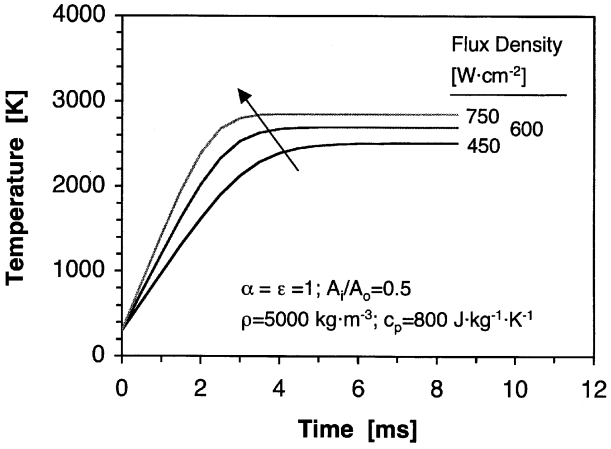

Figure 8. Calculated heating curves for particles with a diameter of 5 μm as a function of the flux density; for details see text.

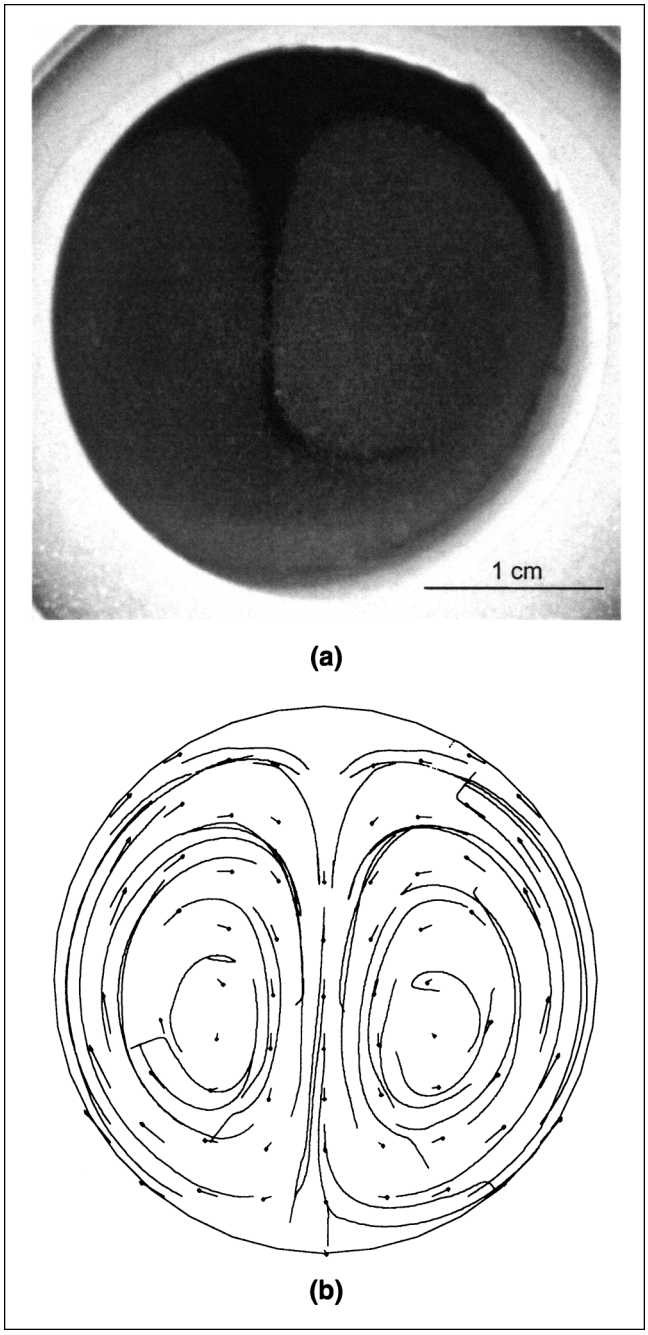

Figure 9. Gas/powder suspension in the CAIRO reactor.

(a) Photograph of the flow pattern in the high-temperature zone, and (b) CFD simulation showing the observed phenomena.

Table 2. Conversion [in %] of Mixed Iron Oxides and Manganese Oxide Under Nitrogen*

Reaction	Flux Density** [W·cm^{-2}]	Mean Conversion† [%]	Reduction Temperature†† [K]
1/3 $(Fe_{0.9}Mn_{0.1})_3O_4 \rightarrow (Fe_{0.9}Mn_{0.1})O$	340–495	15.7	2,050
1/3 $(Fe_{0.9}Mg_{0.1})_3O_4 \rightarrow (Fe_{0.9}Mg_{0.1})O$	232–410	20.4	2,120
1/3 $Mn_3O_4 \rightarrow MnO$	314	23.3	n.d.‡

*The nitrogen flow rate through the solar reactor was 12.5 L·min^{-1}. The residence time of the particles was estimated to be between 40 and 52 ms.
**The range represents the variation between the experiments. Individual values were measured at the entrance plane of the CPC and averaged over a circle with a diameter of 10 mm.
*†The 95% confidence interval was determined to be 5.5% (see text).
††Temperature required to achieve 50% conversion under a flow of N_2 within 10 s in an electrically heated graphite cuvette (Nüesch, 1994).
‡Not determined.

heating zone, the composite refractory wall construction provided a stable high-temperature zone with high tolerance against thermal shocks and thermal gradients. The only part that needed to be replaced after six startups was the first of the three zirconia elements, because it reacted slowly with oxide material, which finally led to melting. Visual observation of the particle cloud through the aperture confirmed the formation of a stable flow pattern. The particle cloud, however, did not move through the tube in a plug-flow-like manner, but formed two symmetrical rolling flows (see Figure 9a). We explain this behavior with the buoyancy effect along the hot walls. The observation could be reproduced by CFD calculations for positions in the middle of the high-temperature zone (see Figure 9b).

Chemical investigations on the reduction behavior of the oxides were initiated with solar experiments under nitrogen. Table 2 lists the yield for two mixed iron oxides and manganese oxide. Earlier experiments in an electrically heated graphite cuvette showed that the reduction of $(Fe_{0.9}Mn_{0.1})_3O_4$ under a N_2 flow requires temperatures of at least 2,050 K (Nüesch, 1994). The presence of the reduced form in the reacted samples indicates that the particles were exposed to these temperatures at least. The studies on the influence of the oxygen partial pressure are difficult to quantify. Solar experiments under atmospheres with 2 and 20% oxygen, respectively, did not produce samples that contained the reduced form. We do not believe that these results are due to the expected increase of the reduction temperature. We expected at least to observe the reduction of Mn_3O_4 to MnO. Solar experiments with bulk samples (200 mg) showed that the reduction of Mn_3O_4 under air and nitrogen proceeds at comparable temperatures of 2,100 to 2,200 K. The different oxygen partial pressure mainly influences the extent of the MnO formation (Frey et al., 2001).

The reason for the absence of the reduced form was revealed by high-temperature powder X-ray diffractometry and thermogravimetry. They showed that samples from solar experiments under air contained up to 60 mol % of a maghemite-type phase γ-$(Fe_{0.9}Mn_{0.1})_2O_3$ (see Table 3). This phase is formed either by the oxidation of wustite-type or spinel-type iron oxides at temperatures as low as 500 K (Schwertmann and Cornell, 2000), but not higher than 1,200 K (Pattanayak et al., 1990). We therefore conclude that the particles were subject to low-temperature oxidation downstream of the high-temperature zone and that the quenching was not sufficient to prevent particles from reoxidation. Further evidence for insufficient quenching is provided by the analysis of sample material taken from the water-cooled backside of the CPC where efficient cooling is ensured. Samples from reductions of Mn_3O_4 under air taken from this place contained up to 15 mol % MnO, while samples collected on the filter did not contain any MnO.

From the viewpoint of material development, it is noticeable that the experiments with $(Fe_{0.9}Mg_{0.1})_3O_4$ produced the highest yield of the reduced form under N_2 and the least amount of the oxidized form under air. It appears that Fe-Mg-oxides are less sensitive to oxidation than the corresponding $(Fe_{0.9}Mn_{0.1})_3O_4$. Further investigations on this subject are encouraged.

Exposure of the particles to concentrated solar radiation not only induced chemical use, but also affected the morphology and the size of the particles. Figure 10a displays the SEM micrograph of $(Fe_{0.9}Mn_{0.1})_3O_4$ prior to its use in the solar reactor CAIRO. We recognize primary platelike particles with a size of about 0.5 μm, which form conglomerates with a size of at least 1 μm. The displayed morphology is characteristic for this type of compound. Determination of the particle-size distribution by laser diffraction yielded a

Table 3. Chemical Composition [in mol %*] of Spinel-Type Samples Reacted in Air and Collected on the Filter**

Starting Material	Flux Density† [W·cm^{-2}]	1/3 $(Fe_{0.9}Me_{0.1})_3O_4$ [mol %]	1/2 γ-$(Fe_{0.9}Me_{0.1})_2O_3$ [mol %]
1/3 $(Fe_{0.9}Mn_{0.1})_3O_4$	440	41.6††	58.5
1/3 $(Fe_{0.9}Mg_{0.1})_3O_4$	371	76.6††	23.4

*See text for details.
**The air flow rate through the solar reactor was 12.5 L·min^{-1}. The residence time of the particles was estimated to be between 40 and 52 ms.
†Measured at the entrance plane of the CPC and averaged over a circle with a diameter of 10 mm.
††The 95% confidence interval was determined to be 5.5% (see text).

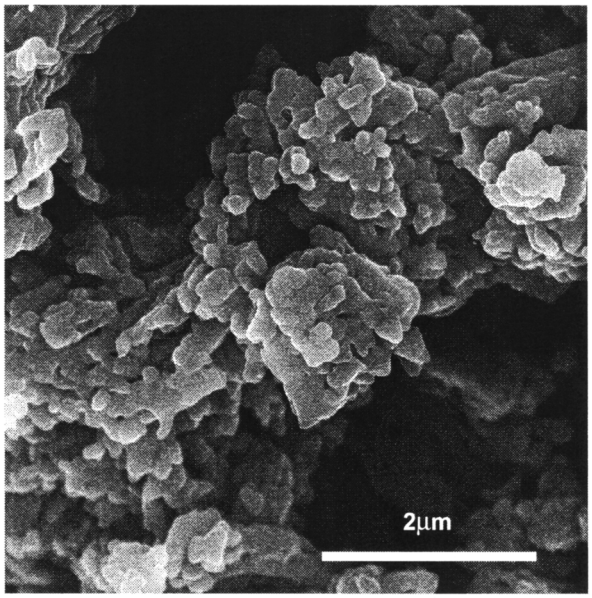

(a)

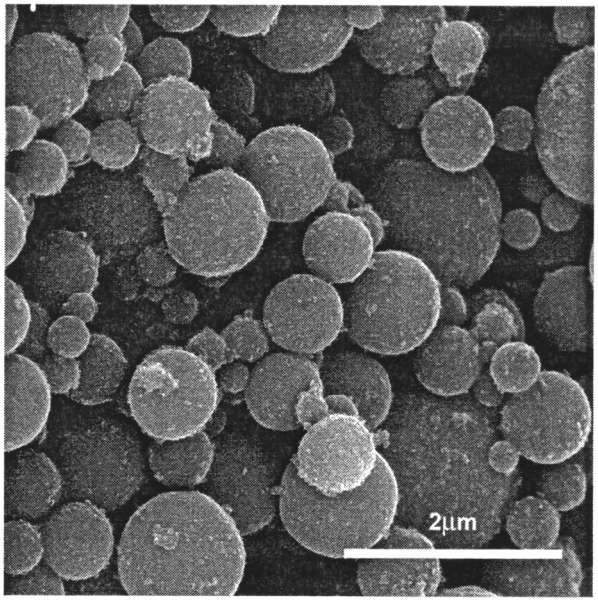

(b)

Figure 10. Scanning electron micrograph (SEM) of $(Fe_{0.9}Mn_{0.1})_3O_4$.

(a) Before the experiments, and (b) after the experiment under an oxygen partial pressure of 20 mbar.

median of 7 μm. This latter result suggests that the conglomerates do not completely separate in the dispersing agent ethanol. Figure 10b shows that heating caused the formation of regular-shaped spherical particles with a typical diameter below 1 μm. This figure is in good agreement with the median of 0.4 μm as it was measured by laser diffraction. The formation of regular-shaped spheres proves that the particles were exposed to temperatures near or above the melting point (approximately 1,900 K), and more importantly, that the particles in the cloud did not coalesce. This observation is important when particle-cloud reactors are discussed for preparing materials with specific properties, for example, high chemical reactivity or good flow behavior.

The characterization of the solar chemical reactor CAIRO was completed with an uncertainty analysis. Since the experimental conditions and the chemical reactions are comparable for all the solar experiments considered, the data for the reduction of $(Fe_{0.9}Mn_{0.1})_3O_4$ under nitrogen (see Table 2) were used to estimate the typical stochastic contribution to the uncertainty. The 95% confidence interval for the mean chemical conversion of 15.7% was calculated to be 5.6%. The uncertainty is attributed in part to variations of the solar flux density. Visually observed spontaneous fluctuations of the particle feeding and the flow pattern seem more important. Fixed errors, for example, related to sample analysis techniques, turned out to be insignificant. The 95% confidence interval corresponds to 35% of the actual mean conversion and agrees well with similar values of 21 to 43% reported by Möller and Palumbo (2001a). These analyses indicate that an uncertainty interval in the range of 20 to 40% is characteristic for experiments with solar chemical reactors and the periphery attached to them.

Development of an alternative reactor outlet

An alternative reactor outlet was developed and tested to achieve a sufficiently fast quench necessary for very oxygen-sensitive materials such as iron oxides. It consists of a central tube positioned in front of the aperture. The gas/solid suspension is removed through this tube (see Figure 11). A similar central reactor outlet had previously been successfully implemented in another volumetric gas/particle solar reactor (Ganz et al., 1999). In combination with a water-spray quench unit, it allowed the harvesting of oxygen-sensitive materials even with air as the auxiliary gas. Furthermore, the experiments demonstrated that placing the outlet tube in front of the aperture has a threefold benefit with regard to both the improved conversion of the incident solar radiation and to increased maximum working temperatures: (1) Most solar concentration systems provide a radiation field with a 3-D flux distribution where the flux densities increase from the

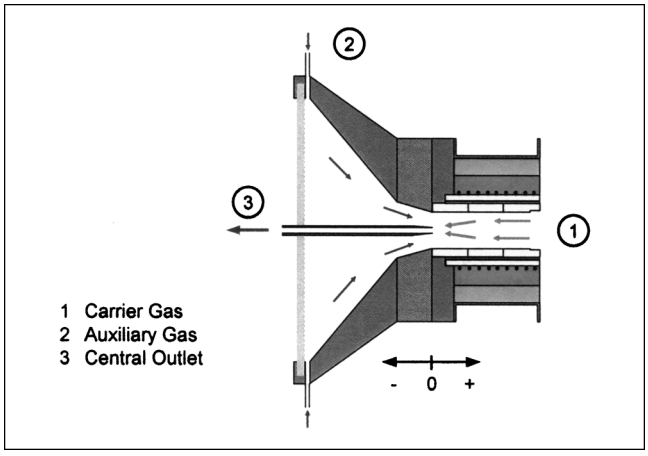

Figure 11. Front part of the solar reactor CAIRO with central outlet.

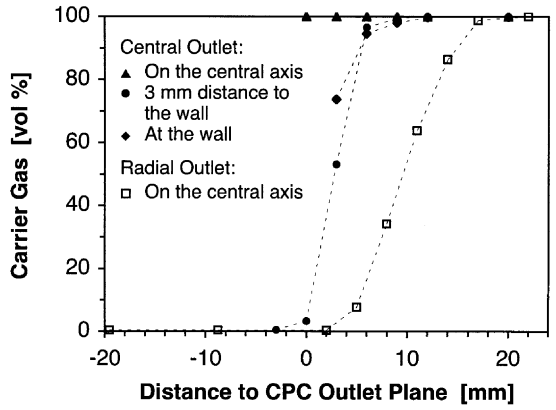

Figure 12. Carrier gas concentration profile in the region of the CPC for the modified reactor outlet (solid symbols).

The concentration profile for the original outlet is added for comparison (open symbols). All measurements were conducted at room temperature.

periphery toward the center (see Figure 6). Placing the outlet tube in the center of the aperture forces the particles to pass first through the low-intensity zone and then through the high-intensity region. In doing this, the particle temperature rises with the radiation intensity, and the energy transfer is most efficient. (2) Visual observation during solar experiments gave evidence that the implementation of the central outlet tube produced a plug-flow-like behavior with smaller convective heat losses to the carrier gas and the reactor walls, respectively, than did the earlier observed well-stirred flow regime. (3) The heat balance also showed that the central outlet tube reduced penetration of auxiliary gas into the high-temperature zone of that solar reactor. Based on these results, the front part of the CAIRO reactor was redesigned, and the new central outlet tube was implemented as sketched in Figure 11. The modified reactor was built from Perspex, and characterization of the flow pattern was conducted at room temperature only. Figure 12 gives strong evidence that the flow pattern in the region of the aperture can be markedly improved. The penetration depth of auxiliary gas into the high-temperature zone is reduced by 8 to 12 mm and the transition zone between carrier gas and auxiliary gas is narrowed. We therefore expect higher maximum working temperatures and a better control of the gas composition in the aperture (when carrier gas and auxiliary gas, respectively, are different). While the expected benefits are obvious, the technical feasibility of the outlet tube needs further evaluation. Since the outlet tube is exposed to concentrated solar radiation, active cooling is required, for example, by the flow of cooling water through a double-walled tube. However, to build such a central outlet tube for the CAIRO reactor is quite a challenge, since the outer diameter should not exceed 0.9 cm to limit shading losses to approximately 10% (Ganz et al., 1999).

Summary and Conclusions

Experiments proved that the solar chemical reactor CAIRO is well suited for semiquantitative chemical reactivity studies on very small particles with typical reaction times of a few tens of milliseconds at temperatures above 2,000 K. Two key features of the solar reactor are a compound parabolic concentrator (CPC) and a high-temperature reaction zone with wall temperatures around 2,000 K. The CPC provides the required flux densities of 450 $W \cdot cm^{-2}$ on 85% of the cross section to achieve stagnation temperatures of 2,500 K. Hot walls reduce heat losses of reacting particles and enable them to reach temperatures close to calculated stagnation temperatures even with optically thin powder clouds with mass load ratios as low as 0.02 kg per kg carrier gas. A third feature is the quartz window that allows experiments under defined atmospheres. Continuous and stable operation of the solar reactor was possible, since particle deposition on the CPC or on the window could be avoided by an appropriate choice of carrier and auxiliary gas flow rates. However, such specific flow requirements limit the variation of the particle residence time because gas flow and residence time are strongly interrelated. Sample temperatures can only be inferred from the occurrence of the chemical reaction and from calculations of stagnation temperatures.

Solar experiments with the CAIRO reactor showed that the uncertainty in chemical conversion is dominated by a stochastic contribution from the solar experimentation, in particular from the solar chemical reactor and its periphery. Chemical analyses of the products revealed that quenching must be improved for studying reactions with highly reactive products under air. Investigations with a modified version of the CAIRO reactor at room temperature and results from another solar powder cloud reactor indicate that a central outlet tube in front of the aperture is a promising alternative.

Although the experimental solar reactor CAIRO was devised for studies on metal oxides, it is apparently also well suited for high-temperature reactivity studies on other condensed-phase materials such as high-performance ceramics; thus, it exemplifies the close relationship between energy research and material science.

Acknowledgments

Continuous financial support from the Swiss Federal Office of Energy (BFE) is gratefully acknowledged. The authors thank D. Wuillemin for constructing the solar reactor, A. Frei for experimental support and chemical analyses, V. Shklover for taking the SEM photographs, and R. Palumbo for valuable discussions.

Literature Cited

Anonymous, "CFX-F3D Flow Solver User Guide," AEA Technology, Harwell, UK (1995).

Barin, I., *Thermochemical Data of Pure Substances*, VCH, Weinheim, Germany (1995).

Ehrensberger, K., P. Kuhn, V. Shklover, and H. R. Oswald, "Temporary Phase Segregation Processes During the Oxidation of $(Fe_{0.7}Mn_{0.3})_{0.99}O$ in N_2-H_2O Atmosphere," *Solid State Ionics*, **90**, 75 (1996).

Frey, T., E. Steiner, D. Wuillemin, and M. Sturzenegger, "TREMPER—A Versatile Tool for High-Temperature Chemical Reactivity Studies under Concentrated Solar Radiation," *J. Sol. Energy Eng.*, **123**, 147 (2001).

Funk, J. E., "Thermochemical Production of Hydrogen via Multistage Water Splitting Processes," *Proc. Hydrogen Energy Fundam. Symp. Proc.*, Miami Beach, FL, p. S2-3 (1975).

Ganz, J., "Entwicklung von Gas-Feststoff-Reaktoren zur solarthermischen Metalloxid-Reduktion," PhD Thesis, Eidgenösssische Technische Hochschule ETHZ, Zürich, Switzerland (1996).

Ganz, J., E. Steiner, and M. Sturzenegger, "Powder Cloud Reactors —An Attractive Concept to Run Solar High-Temperature Reactions," *J. Phys. IV France*, **9**(3), 361 (1999).
Hunt, A. J., "Solar Radiant Heating of Small Particle Suspensions," Rep., Lawrence Berkeley Laboratory, University of California, Berkeley (1982).
Hunt, A. J., J. Ayer, P. Hull, R. McLaughlin, F. Miller, J. E. Noring, R. Russo, and W. Yuen, "Solar Radiant Heating of Gas-Particle Mixtures," FY 1984 Summary Rep., Lawrence Berkeley Laboratory, University of California, Berkeley (1986).
Kuhn, P., K. Ehrensberger, E. Steiner, and A. Steinfeld, "An Overview on PSI's High-Temperature Solar Chemistry Research," *Proc. ASME Int. Solar Energy Conf.*, Maui, HI, p. 375 (1995).
Möller, S., and R. Palumbo, "The Development of a Solar Chemical Reactor for the Direct Thermal Dissociation of Zinc Oxide," *J. Sol. Energy Eng.*, **123**(2), 83 (2001a).
Möller, S., and R. Palumbo, "Solar Thermal Decomposition Kinetics of ZnO in the Temperature Range 1950–2400 K," *Chem. Eng. Sci.*, **56**, 4505 (2001b).
Nakamura, T., "Hydrogen Production from Water Utilizing Solar Heat at High Temperatures," *Sol. Energy*, **19**, 467 (1977).
Nüesch, P., "Untersuchungen zur thermischen Reduktion von Eisen-Mischoxiden mit Spinellstruktur bei Temperaturen bis zu 2000°C," Diploma Thesis, Univ. Zürich, Zürich, Switzerland (1994).
Palumbo, R., J. Lédé, O. Boutin, E. Elorza Ricart, A. Steinfeld, S. Möller, A. Weidenkaff, E. A. Fletcher, and J. Bielicki, "The Production of Zn from ZnO in a High-Temperature Solar Decomposition Quench Process," *Chem. Eng. Sci.*, **53**(14), 2503 (1998).
Pattanayak, J., V. S. Rao, and H. S. Maiti, "Effect of Iron Concentration on the Thermal Behaviour of γ-Mn_2O_3," *Thermochim. Acta*, **160**, 233 (1990).
Raghunathan, K., A. Ghosh-Dastidar, and L.-S. Fan, "High Temperature Reactor System for Study of Ultrafast Gas-Solid Reactions," *Rev. Sci. Instrum.*, **64**(7), 1989 (1993).
Ries, H., and M. Schubnell, "The Optics of a Two-Stage Solar Furnace," *Solar Energy Mater.*, **21**, 213 (1990).
Schwertmann, U., and R. M. Cornell, *Iron Oxides in the Laboratory*, Wiley-VCH, Weinheim, Germany (2000).
Sizmann, R. L., "Solar Radiation Conversion," *Solar Power Plants*, C. J. Winter, R. L. Sizmann, and L. L. Vant-Hull, eds., Springer-Verlag, Berlin (1991).
Steinfeld, A., and M. Schubnell, "Optimum Aperture Size and Operating Temperature of a Solar Cavity-Receiver," *Sol. Energy*, **50**(1), 19 (1993).
Steinfeld, A., P. Kuhn, A. Reller, R. Palumbo, J. Murray, and Y. Tamaura, "Solar-Processed Metals as Clean Energy Carriers and Water-Splitters," *Int. J. Hydrogen Energy*, **23**(9), 767 (1998).
Sturzenegger, M., and P. Nüesch, "Efficiency Analysis for a Manganese Oxide Based Thermochemical Cycle," *Energy*, **24**(3), 959 (1999).
Sturzenegger, M., J. Ganz, P. Nüesch, and T. Schelling, "Solar Hydrogen from Manganese Oxide Based Thermochemical Cycle," *J. Phys. IV France*, **9**(3), 331 (1999).
Tofighi, A., "Contribution à l'Étude de la Decomposition des Oxydes de fer au Foyer d'un Four Solaire," PhD Thesis, L'institut national polytechnique de Toulouse, Toulouse, France (1982).
Tofighi, A., and F. Sibieude, "Dissociation of Magnetite in a Solar Furnace for Hydrogen Production. Tentative Production Evaluation of a 1000 kW Concentrator from Small Scale (2 kW) Experimental Results," *Int. J. Hydrogen Energy*, **9**(4), 293 (1984).
Tschudi, H. R., and M. Schubnell, "Measuring Temperatures in the Presence of External Radiation by Flash Assisted Multiwavelength Pyrometry," *Rev. Sci. Instrum.*, **70**(6), 2719 (1995).
Welford, W. T., and R. Winston, *High Collection Nonimaging Optics*, Academic Press, San Diego (1989).
Wickham, D. G., "The Chemical Composition of Spinels in the System Fe_3O_4-Mn_3O_4," *J. Inorg. Nucl. Chem.*, **31**, 313 (1969).
Yuen, W. W., F. J. Miller, and A. J. Hunt, "Heat Transfer Characteristics of a Gas-Particle Mixture Under Direct Radiant Heating," *Int. Commun. Heat Mass Transfer*, **13**, 145 (1986).

Manuscript received Oct. 3, 2002, and revision received Apr. 17, 2003.